Amygdala GABA Neurons: Gatekeepers of Stress and Reproduction

Author Information

Junru Yu,[1,†] Saeed Farjami,[2,3,†] Kateryna Nechyporenko,[2,3,†] Xiao Feng Li,[1] Hafsa Yaseen,[1,4] Yanyan Lin,[1] Jinbin Ye,[1] Owen Hollings,[1] Ross de Burgh,[1] Kevin T. O'Byrne,[1,*] Krasimira Tsaneva-Atanasova,[2,3,5,*] Margaritis Voliotis,[2,3,*]

Affiliations

[1]Department of Women and Children's Health, School of Life Course and Population Sciences, King's College London, Guy's Campus, London SE1 1UL, UK, [2]Department of Mathematics and Statistics, [3]Living Systems Institute, [4]Biological Sciences, University of Missouri, Columbia, MO 65211-7400 and [5]EPSRC Hub for Quantitative Modelling in Healthcare, University of Exeter, Stocker Road, Exeter EX4 4PY, UK

Abstract

Stress can disrupt menstrual cycles, cause infertility, and lead to other reproductive disorders. The posterodorsal medial amygdala (MePD) processes stress signals and regulates the gonadotropin-releasing hormone (GnRH) pulse generator through GABAergic inhibitory projections to the hypothalamus. However, how stress is processed in the MePD - especially involving its dense GABAergic and Urocortin-3 (UCN3) neurons - remains poorly understood.

In this study, we combine *in vivo* GRadient-INdex (GRIN) lens mini-endoscopic calcium imaging (to track neuronal activity), optogenetics, clustering analysis, and computational modeling to investigate MePD circuitry. Our findings reveal two anti-correlated GABAergic sub-populations in the MePD that dictate responses to both UCN3 neuron stimulation and restraint stress. Our computational modeling suggests that mutual inhibition between these GABAergic groups drives this anti-correlated activity and predicts how these interactions shape downstream responses to stimulation of GABAergic and UCN3 neurons.

We test these predictions using optogenetics and confirm that GABAergic neurons operate downstream of the UCN3 population, playing a crucial role in transmitting UCN3 signals to regulate luteinizing hormone (LH) pulse frequency. Our study is the first to show how GABAergic neurons in the amygdala mediate stress effects on reproductive health, uncovering key neural mechanisms linking emotional and reproductive functions.

31 ## Introduction

32 Successful reproduction requires normal function of a neural oscillator, the gonadotropin-releasing
33 hormone (GnRH) pulse generator, that drives the pulsatile release of gonadotropic hormones,
34 luteinizing hormone (LH) and follicle stimulating hormone (FSH) to control ovulation and
35 spermatogenesis. This oscillator comprises Kisspeptin neurons co-expressing Neurokinin-B (NKB)
36 and Dynorphin A (acronym KNDy) in the hypothalamic arcuate nucleus (ARC). The KNDy neural
37 network not only provides the essential episodic stimulatory kisspeptin signal to the GnRH neurons,
38 but receives diverse afferent inputs and hence is a hub for integrating various internal and external
39 cues that regulates reproductive function[1,2]. The most common cause of insufficient GnRH drive is
40 functional, that is, due to neuroendocrine effects of psychological and behavioral variables.

41 The amygdala, a part of the limbic brain typically associated with emotions and anxiety, has strong
42 projections to the KNDy system[1,2]. The medial amygdala, and more specifically its posterodorsal
43 subnucleus (MePD), has been shown to be a robust upstream regulator of GnRH pulse generator
44 frequency[3–5], pubertal timing[6,7], sociosexual behaviour[8,9], anxiety[8] and psychological stress-induced
45 suppression of pulsatile LH secretion[10,11].

46 In the MePD, the majority of neurons are GABAergic, accounting for a substantial portion of its
47 projections, many of which target important hypothalamic centers involved in reproduction[12–14],
48 including the KNDy neurons and optogenetic stimulation of the latter suppress LH pulsatility[11].
49 Moreover, chemogenetic inhibition of GABA neurons in the MePD can reverse the inhibitory effect of
50 psychogenic stress on LH pulsatility[11], suggesting an involvement of GABAergic signaling in the
51 stress-induced suppression of pulsatile LH secretion. Although the precise way in which the MePD
52 GABAergic neurons influence LH pulsatility is not fully understood, it has been suggested that they
53 interact with the stress neuropeptide urocortin-3 (UCN3) neurons to modulate or reinforce stress-
54 induced suppression of LH pulse frequency[10].

55 UCN3, part of the corticotropin-releasing factor (CRF) superfamily and selective for CRF type 2
56 receptors (CRFR2)[15], is highly expressed in the MePD[10,16]. Furthermore, UCN3 neurons in the
57 MePD mediate psychosocial stress-induced suppression of the GnRH pulse generator and
58 corticosterone secretion, thus play a central role in the interaction between the reproductive and
59 stress axes[10,17]. Previously we have shown that intra-MePD GABA antagonism can reverse UCN3-
60 induced LH pulse suppression[17], suggesting that GABA acts downstream of UCN3 signalling within
61 the MePD. However, the local neural circuitry within the MePD mediating stress related information
62 to the GnRH pulse generator remains to be established.

63 Here, we employed GRadient INdex (GRIN) lens mini-endoscopy to monitor and compare the
64 calcium activity of GABA neurons at single-cell resolution under acute psychological stress or
65 optogenetic stimulation of UCN3 neurons. Clustering analysis of the observed calcium transients
66 uncovered two distinct GABAergic sub-populations exhibiting anti-correlated activity. To explore the
67 functional role of these two sub-populations and unpick the mechanisms driving their anti-correlated
68 activity, we build upon our previously developed MePD circuitry mathematical modeling framework[5].
69 Our modeling reveals that mutual inhibitory interactions between the GABAergic populations are
70 sufficient to drive anti-correlated activity and predicts a complementary inhibitory effect of GABA and
71 UCN3 signaling on the frequency of the GnRH pulse generator, which we tested by applying Cre/Flp
72 recombinase intersectional strategies to selectively target and manipulate heterogeneous MePD
73 neuronal populations[11] . Hence, by uncovering precise interactions between distinct sub-populations
74 of MePD GABAergic neurons and UCN3 neurons in transmitting stress signals to the GnRH pulse
75 generator, we provide critical and previously unknown insights into the neural circuitry driving stress-
76 induced reproductive dysfunction. This discovery significantly advances our understanding of how
77 emotional stress directly impacts reproductive health and identifies potential neural targets for
78 therapeutic intervention in stress-related reproductive disorders.

Results

Dynamic reconfiguration of MePD GABA neuronal networks during selective optogenetic stimulation of urocortin-3 (UCN3) neurons and restraint stress

To investigate how the posterodorsal subnucleus of the medial amygdala (MePD) processes stress signals and to understand the role of GABAergic and UCN3 neurons in this process, we employed *in vivo* calcium imaging using GRadient INdex (GRIN) mini-endoscopy. A cohort of six female UCN3-Cre::VGAT-Flpo transgenic mice were injected with a viral mixture containing pAAV-Syn-Flex-rc[Chrimson-tdTomato] and pAAV-EF1a-fDIO-GCaMP6s. This intersectional viral strategy enabled dual functionality: (i) optogenetically stimulating MePD UCN3 neurons via Chrimson; and (ii) detecting calcium activity in MePD GABAergic neurons using GCaMP6s (Fig. 1**A**). GRIN lenses were surgically implanted at the same location as the viral injection, enabling imaging of calcium activity with single-neuron resolution.

Two series of experiments were conducted to assess GABAergic responses under distinct conditions. First, to assess the role of UCN3 neurons in recruiting GABAergic response, baseline calcium activity from MePD GABAergic neurons was recorded for 2 min, followed by 2 min of recording during optogenetic stimulation of UCN3 neurons (Fig. 1**A**). Optogenetic stimulation was delivered in a discontinuous pattern, 5 seconds on, 5 seconds off, with a light-pulse frequency of 10 Hz during the ‘on’ periods (10-ms pulse width, 10 mW power, and 532 nm wavelength). To further characterize the GABAergic response to acute stressors, baseline calcium activity of GABAergic neurons was recorded for 2 min, followed by 2 min of recording while the animals were exposed to restraint stress (Fig. 1**A**).

The dynamic GABAergic response to optogenetic stimulation of UCN3 neurons and restraint stress was summarized in functional terms using pairwise (neuron-neuron) association matrices, constructed using the signed lagged cross-correlation (SLxCorr) metric. SLxCorr captures the correlation between the activity of two neurons while accounting for both temporal lags and the sign (positive or negative) of their association (see Methods). Hence, SLxCorr matrices represent the

105 MePD GABAergic response as a set of interconnected nodes (neurons) with connections weighted
106 by their functional interactions (Fig. 1**H**&**I**). Our analysis reveals significant differences in the
107 functional connectivity of the GABAergic network in both experimental conditions (Fig. 1**J**) that we
108 also confirm using an alternative measure of pairwise association, namely covariance (see Methods
109 and Supplementary Fig. 1). These results robustly indicate that the GABAergic population in the
110 MePD plays a pivotal role in processing stress signals, such as those induced by restraint stress.
111 Furthermore, our findings suggest that UCN3 neurons may serve as a critical relay, transmitting
112 stress-related information to the GABAergic population.

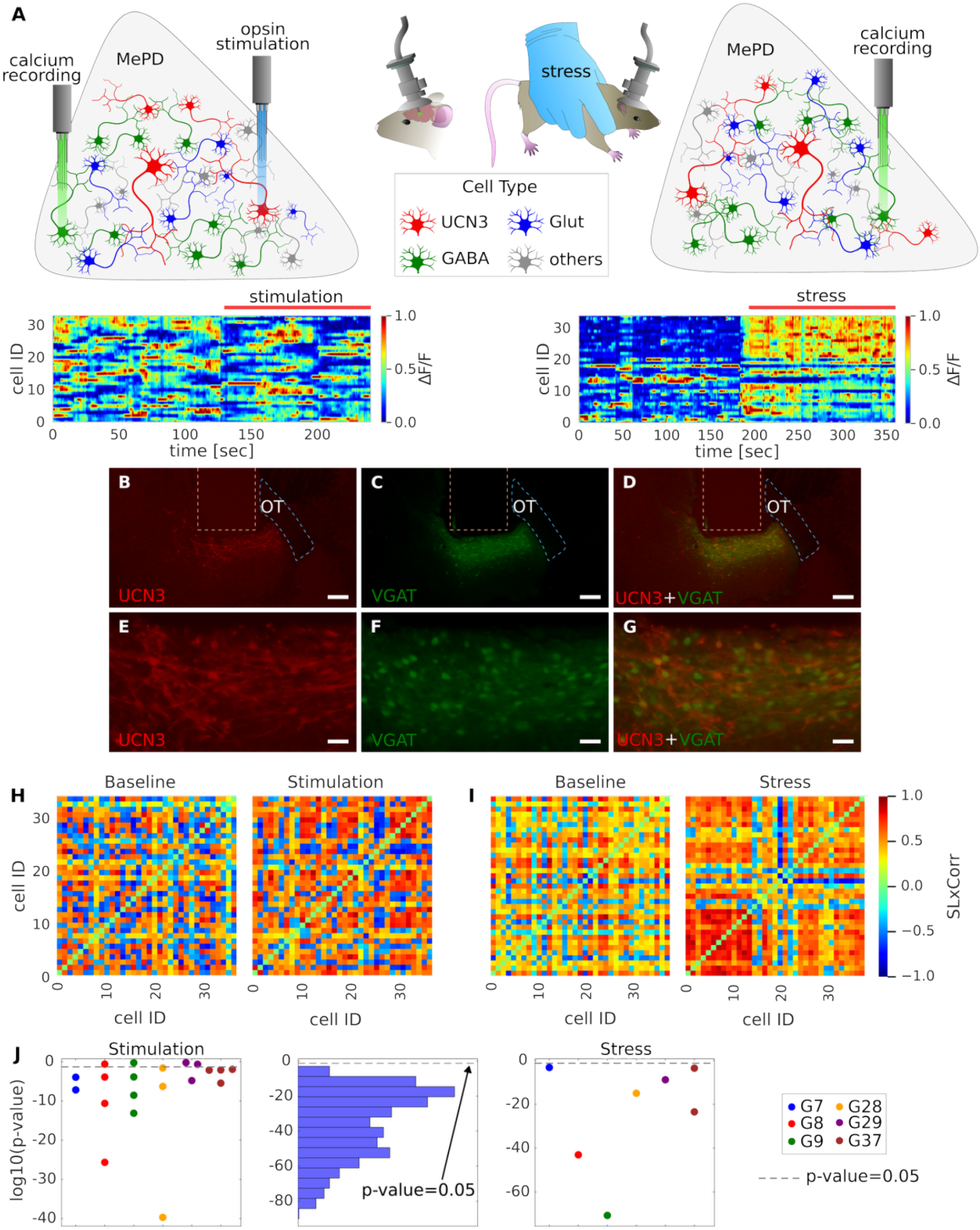

Figure 1: **Functional connectivity of GABAergic neurons in posterodorsal medial amygdala (MePD) reconfigures in response to optogenetic stimulation of urocortin-3 (UCN3) neurons or acute restraint**

116 **stress**. (**A**) Schematic diagram of the experimental design for stimulating MePD UCN3 neurons and
117 simultaneously imaging calcium activity from MePD GABAergic neurons. Heatmaps of calcium activity (ΔF/F)
118 in response to (left) optogenetic stimulation of UCN3 neurons and (right) during restraint-induced stress. (**B**-**G**)
119 Representative photomicrographs of the MePD from a UCN3-Cre::VGAT-Flpo mouse injected with pAAV-Syn-
120 Flex-rc+pAAV-EF1a-fDIO-GCaMP6s. (**B**&**E**) Red fluorescence (tdTomoato) labels UCN3 neurons expressing
121 Chrimson-tdTomato, (**C**&**F**) green fluorescence labels GABAergic neurons, and (**D**&**G**) red and green signals
122 merged. (**H**&**I**) Functional connectivity in the GABA populations was quantified using signed lagged cross-
123 correlation (SLxCorr). (**J**) Functional connectivity weights show a statistically significant difference between
124 the baseline period and subsequent UCN3 stimulation or restraint stress across animals, assessed via
125 Kolmogorov-Smirnov tests for each animal trial and using Fisher's method for combining p-values across data
126 sets recorder in different animals (see Methods). Distribution of combined p-values obtained from different
127 combinations of trials (one from each animal) is consistently below the 0.05 confidence level. Scale bars: **B**-
128 **D**, 200 μm; **E**-**G**, 50 μm.

129 **Clustering analysis reveals two functionally distinct GABAegic sub-populations in the MePD**

130 To better understand the functional organization of the GABAergic MePD network during
131 optogenetic stimulation of UCN3 neurons and under restraint stress, we performed clustering
132 analysis of the calcium recordings (time series) from GABAergic neurons.

133 The Signed Lagged Cross-Correlation (SLxCorr) was transform into a dissimilarity score, based on
134 which we performed hierarchical clustering. Clustering results consistently revealed two functionally
135 distinct cell populations both during optogenetic stimulation of UCN3 neurons and restraint stress
136 (Fig. 2**A**&**C**). Under both conditions, activity between the two clusters appeared highly anti-
137 correlated as illustrated by two representative examples depicted in Fig. 2**B**&**D**. Moreover, we find
138 that clusters are significantly different in size with the smallest cluster accounting on average for
139 35% of all cells (Fig 2**D**&**E**, Supplementary Fig. 2). The robustness of the above finding was also
140 verified using the K-means clustering algorithm and pairwise covariance as an alternative
141 dissimilarity score (see Methods and Supplementary Figs. 3-5).

142 Based on the functional role of the MePD in relaying stress signals to the hypothalamic arcuate
143 nucleus (ARC), our results suggest that the identified GABAergic sub-populations (clusters) could

correspond to distinct populations of GABA interneurons and GABA efferent neurons projecting to the ARC. These projections play a role in regulating the gonadotropin-releasing hormone (GnRH) pulse generator, a key driver of reproductive function[5,11].

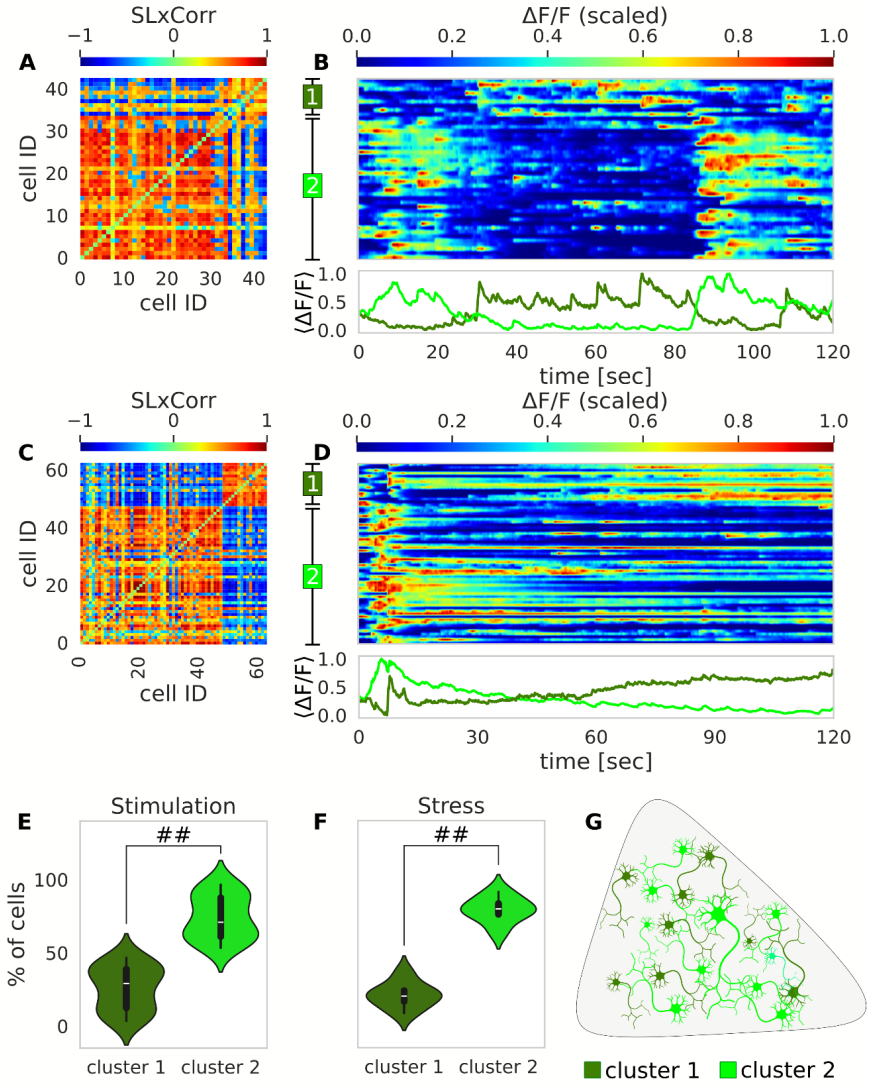

Figure 2: **Clustering identifies two functionally distinct GABAergic sub-populations in the posterodorsal medial amygdala (MePD) both during UCN3 optogenetic stimulation and restraint stress**. Representative example of (**A**) a clustered connectivity matrix and (**B**) associated calcium time-traces of MePD GABA neurons during optogenetic stimulation of UNC3 neurons. Representative examples of (**C**) a clustered connectivity matrix and (**D**) associated calcium activity time-traces of MePD GABA neurons during restraint stress. (**E**&**G)** Relative sizes of the two GABAergic sub-populations identified via clustering analysis. (##: $p<0.001$).

155 **Mutually inhibitory interactions between GABA populations drive anti-correlated activity**

156 To explore the functional role of the two GABAergic sub-populations identified through clustering
157 analysis and unpick the mechanisms driving their anti-correlated activity, we build upon our
158 previously developed MePD circuitry mathematical modeling framework[5]. The model captures the
159 dynamics of intracellular calcium activity in sub-populations of GABA neurons (we refer to them as
160 interneurons and efferent neurons) that interact with a glutamatergic neuronal population (Fig. 3**A**).
161 Glutamate antagonism has been shown to completely block the suppressive effect of MePD UCN3
162 activation on LH pulsatility[17], suggesting a functional importance of glutamatergic neurons in the
163 circuit, hence we keep this neuronal population in the model. To incorporate UCN3 input we include
164 a non-autonomous term in the model informed by recordings of the activity of UCN3 neurons during
165 optogenetic stimulation (see Fig. 3**A** and Methods). The recorded traces exhibit a periodic pattern
166 driven by the experimental stimulation protocol with 5 seconds on, 5 seconds off (see Methods). In
167 the model, we approximated this UCN3 input using a sinusoidal function with roughly 5 seconds on,
168 5 seconds off pattern, driving the populations GABAergic interneurons and the glutamatergic
169 neurons. We parametrize our MePD model to reproduce anti-correlated activity between the two
170 GABA neuronal sub-populations. To achieve this we need to include bi-directional (i.e. mutually
171 inhibitory) GABA interaction in the circuit as well as GABA interneurons self-inhibition (Fig. 3**A**).

172 Next we simulate the effects of stress on the MePD circuit in our parametrized model. UCN3
173 neurons in the MePD have also been shown to mediate psychosocial stress-induced suppression of
174 the GnRH pulse generator[10]. Using our mathematical model, we begin by reproducing experimental
175 observations of GABA activity under an acute (120 seconds) stress intervention (Fig. 3**B**).
176 Experimentally recorded calcium activity of UCN3 neurons during stress intervention is
177 characterized by a fast rise followed by a slow decay (Fig. 3**B**), which we model by taking the
178 difference between two exponential functions, one with a fast and one with a slow time constant
179 (see Methods). The model confirms emergence of anti-correlated behavior between the GABAergic
180 sub-population whereby the activity of GABA interneurons decreases over the stress period, while

181 the activity of the GABA efferent neuron population increases (Fig. 3**B**), supporting the proposed

182 MePD circuit structure (Fig. 3**A**).

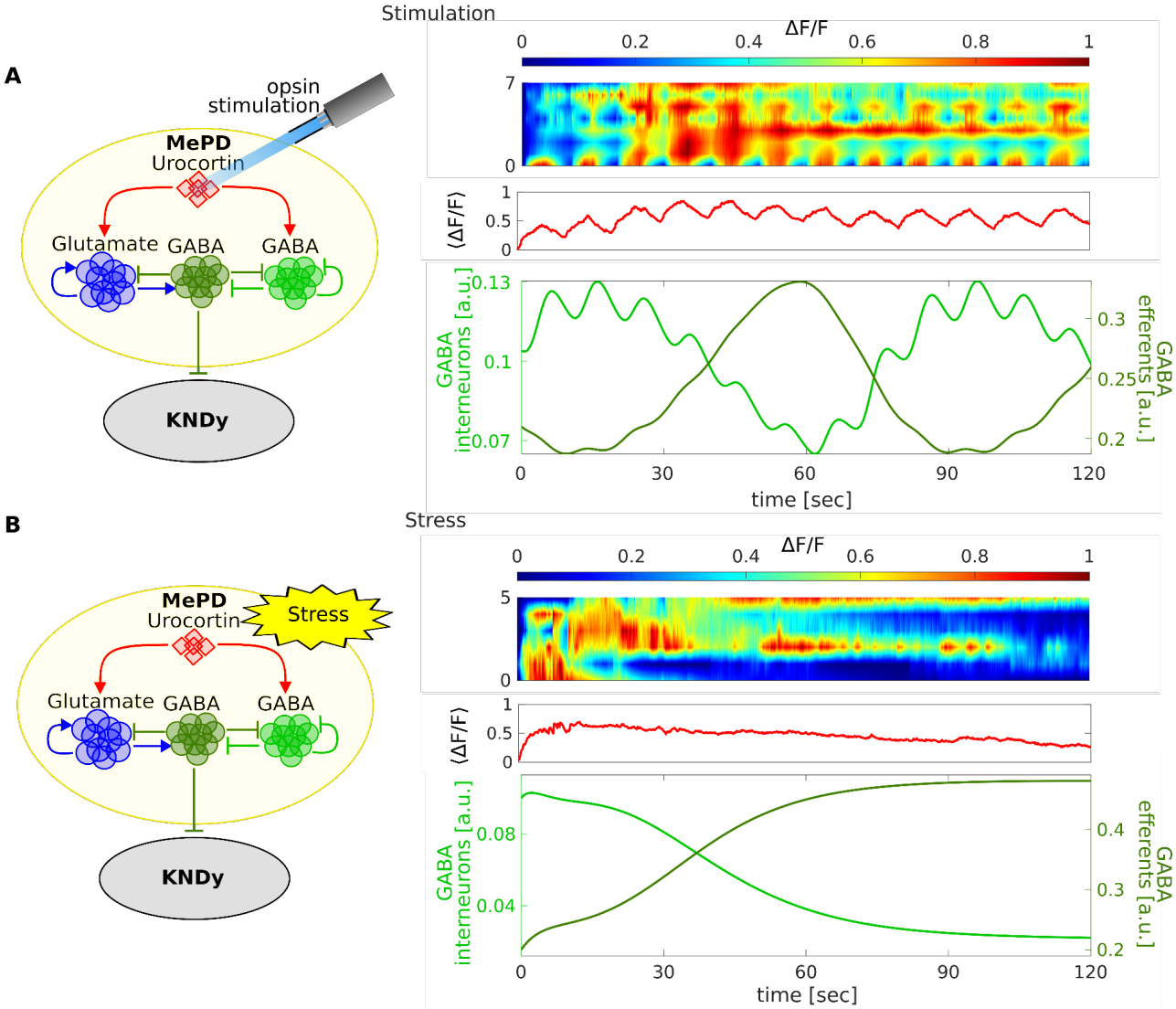

183

184 **Figure 3: *In silico* simulation of the activity in the GABAergic neuronal populations in the MePD under**

185 **the increased excitatory input from UCN3 neurons and under restraint stress.** Schematic on the left

186 represents the MePD neuronal circuit interacting with UCN3, consisting of two GABA populations and a

187 glutamatergic population. (**A**) Calcium time-traces of MePD UCN3 neurons during optogenetic stimulation of

188 UCN3 neurons and corresponding mean activity. Model simulations of the effects of UCN3 optogenetic

189 stimulation supports the emergence of anti-correlated activity in GABAergic sub-populations. (**B**) Calcium

190 time-traces of MePD UCN3 neurons during restraint stress and corresponding mean activity of the UCN3

191 calcium traces during restraint stress with corresponding mean activity. Simulations of the MePD circuit under

192 the effects of stress also support anti-correlated GABAergic sub-populations' activity.

193 ***In silico* modeling reveals complementary relationship between MePD GABA and UCN3**
194 **populations**

195 Having shown that MePD model can reproduce anti-correlated activity of two GABA sub-
196 populations, we examine the effects of distinct interventions involving GABA and UCN3 in the MePD
197 on the LH pulses via coupling the model of the MePD circuitry defined in the previous section to our
198 network model of the KNDy population in the arcuate nucleus (ARC)[5,18]. Building on our previous *in*
199 *silico* findings, which suggest that MePD signal integration is mediated predominately by GABAergic
200 projections[5], here we consider only the input from GABA efferent neuron to the KNDy network in
201 order to complete our coupled MePD – KNDy network model. The effects of MePD GABA and
202 glutamate antagonism alone and together with UCN3 stimulation on LH pulsatility have been
203 previously investigated[17]. We calibrate our coupled model parameters by reproducing these effects
204 accordingly (see Supplementary Fig. 6).
205 Next using the calibrated model, we predict that providing a periodic excitatory input (see
206 Supplementary Fig. 7(**A**)), that mimics the effects of optogenetic stimulation of UCN3, leads to the
207 increase in the KNDy inter-pulse interval (IPI) from 15.18 min to 23.97 min due to increased activity
208 in the inhibitory GABAergic input to the KNDy network (Fig. 4**A**).
209 Since MePD has an overwhelming number of GABAergic outputs and interneurons, we are
210 interested in their role in information processing of stress signaling. To this end we provide periodic
211 excitatory input directly to both populations of GABA neurons (see Supplementary Information). This
212 is different to the indirect activation through UCN3 stimulation, as it leads to the increased activity in
213 both GABA subpopulations (Supplementary Fig. 7(**B**)). The resulting effect on the KNDy IPI is an
214 increase from 15.18 min to 42.65 min (Fig. 4**B**).
215 In the model we hypothesize that UCN3 signaling to the KNDy is operating through the GABAergic
216 pathway, hence disrupting GABAergic interactions will suppress UCN3's effects on KNDy. To
217 investigate it we suppress the strength of the GABAergic interactions by 50% and mimic UCN3
218 stimulation by providing excitatory input to the circuit. The model shows that this intervention does

219 not have a significant effect on KNDy IPI, apart from slightly increasing it from 15.18 min to 17.31
220 min (Fig. 4**C** & Supplementary Fig. 7(**C**)).
221 Taken together the above could be summarized as the following set of model predictions along with
222 suggested ways to test them experimentally:

223 1. Optogenetic stimulation modelled via excitation of the MePD UCN3 increases the KNDy IPI
224 15.18 min to 23.97 min. This could be tested experimentally via in vivo optogenetic activation
225 of the MePD UCN3 neuronal populations and simultaneous measurement of LH pulsatility.
226 2. Stimulation of the MePD GABA populations increases the KNDy IPI 15.18 min to 42.65 min.
227 Such a substantial change underscores the critical role of GABAergic signaling in modulating
228 KNDy pulsatility. Experimental confirmation could involve *in vivo* optogenetic activation of the
229 entire MePD GABAergic population accompanied by LH pulsatility measurement.
230 3. Stimulation of the MePD UCN3 with simultaneous suppression of the GABAergic interactions
231 in the MePD does not significantly affect KNDy IPI, changing it from 15.18 min to 17.31 min.
232 This finding suggests that UCN3 effects on the KNDy network are primarily dependent on its
233 interactions with GABA populations. A strategy to verify this hypothesis experimentally could
234 be to stimulate UCN3 non-GABA-expressing neurons in vivo while simultaneously inhibiting
235 non-UCN3 GABAergic neurons and measure LH pulsatility.

236 Finally, we investigate *in silico* the effects of stress on LH pulse dynamics mediated via the MePD.
237 In the restraint-stress experiment it was shown that one GABAergic cluster was active, while the
238 other one was inactive (Fig. 2**D**). By simulating these dynamics (Supplementary Fig. 7(**D**)) in the
239 coupled MePD - KNDy network model we are able to demonstrate that pulses in the KNDy network
240 ceased (Fig. 4**D**). These modeling findings align with published experimental evidence indicating
241 that restraint stress suppresses LH pulsatility[10].

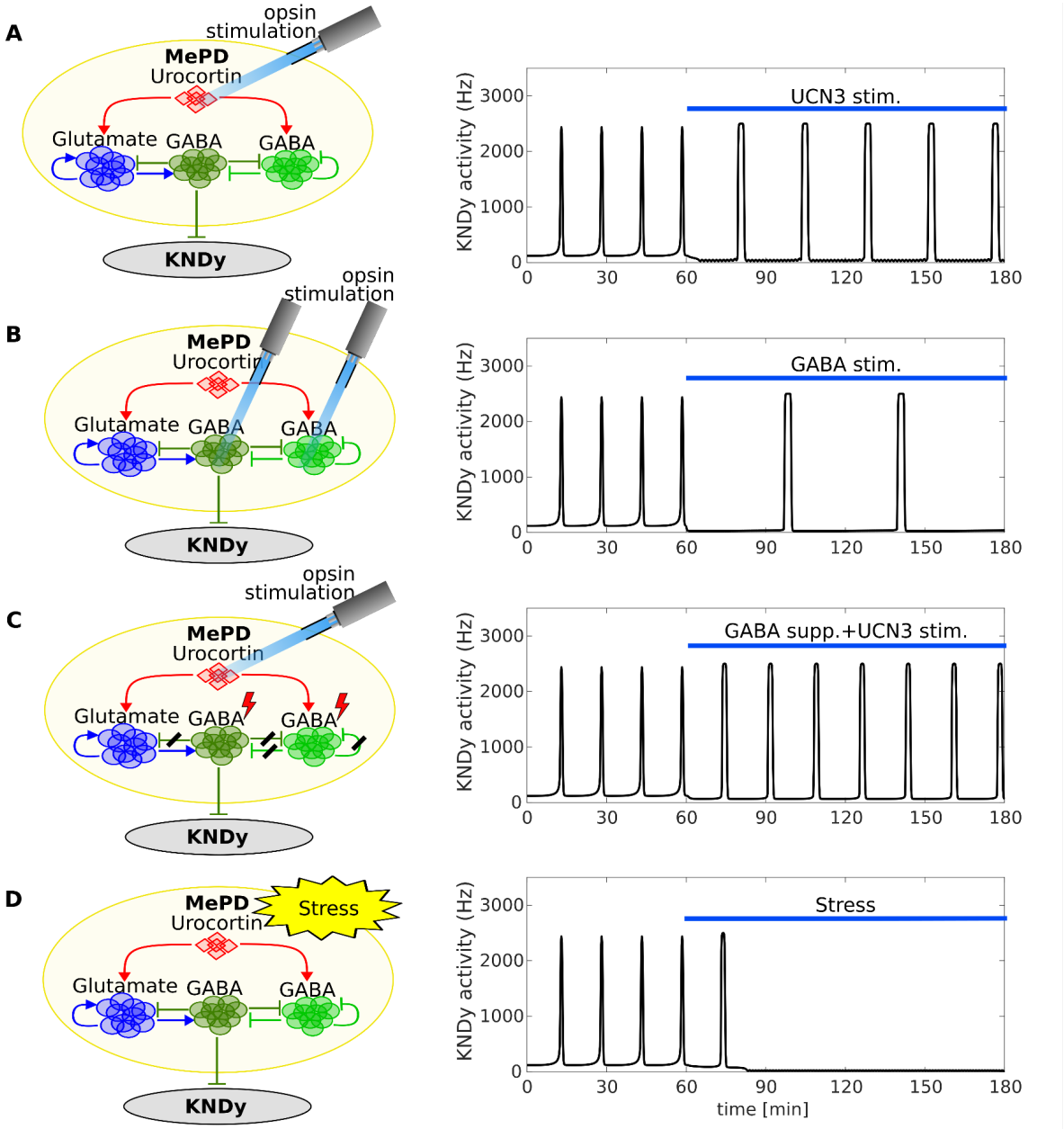

Figure 4: Coupled MePD - KNDy model predictions for the effect of stress and stimulation of UCN3 neurons on GnRH pulse generator activity and hence LH pulsatility. (**A**) Simulation of the optogenetic stimulation of the UCN3 neurons leads to the increase of the KNDy IPI 15.18 min to 23.97 min. (**B**) Optogenetic stimulation of the MePD GABA neurons (providing excitatory input to both GABAergic populations) increases KNDy IPI from 15.18 min to 42.65 min. (**C**) Optogenetic stimulation of the UCN3 neurons and simultaneous inhibition of GABAergic neuronal populations do not significantly affect KNDy IPI, where it changes from 15.18 min to 17.32 min. (**D**) Simulating the effects of stress leads to the cessation of the pulsatile dynamics.

251 **Selective optogenetic stimulation of UCN3 non-GABAergic neurons inhibits pulsatile LH**
252 **secretion in female mice.**

253 We now test experimentally our modeling predictions detailed in the previous section regarding the
254 inhibitory effect of MePD UCN3 activation on LH pulsatility *in vivo* in freely behaving mice. To this
255 end a cohort of UCN3-Cre::VGAT-Flpo transgenic female mice was injected with an AAV-nEF-
256 Con/Foff 2.0-ChRmine-oScarlet viral construct. This intersectional approach enabled conditional
257 expression of channelrhodopsin (ChRmine) in UCN3 neurons not expressing GABA (UCN3 non-
258 GABAergic) (Con/Foff group). Following the viral injection, a unilateral fiber-optic cannula was
259 implanted into the MePD, above the injection site, to facilitate selective activation of the targeted
260 neuronal population.

261 The stimulation protocol consisted of a 60-min control period, followed by 60 min of optogenetic
262 stimulation. Stimulation was delivered, as above, in a pulsed pattern (5 seconds on, 5 seconds off)
263 with a pulse frequency of 10 Hz during the on period (10-ms pulse width, 10 mW power, 532 nm
264 wavelength). Blood samples (5 μL) were collected every 5 min throughout the protocol and used to
265 measure LH levels.

266 Statistical analysis indicated post-stimulation LH inter-pulse intervals differed across the two groups.
267 In the Con/Foff group, the LH inter-pulse interval significantly increased after optogenetic stimulation
268 compared to the control period (15.33 ± 0.83 min vs. 23.75 ± 1.07 min, mean ± SEM, $n = 6$, $p<0.01$;
269 Fig. 5**A**&**D**), validating the first of our modeling predictions. In contrast, the no-stimulation group,
270 which received the Con/Foff viral construct without optogenetic stimulation, showed no significant
271 changes in LH inter-pulse interval (16.11 ± 0.56 min vs. 16.70 ± 0.96 min, $n = 3$, $p > 0.05$; Fig.
272 5**B**&**D**). Similarly, in a separate cohort of mice injected with a control virus (DIO-EYFP), optogenetic
273 stimulation resulted in no significant differences in LH inter-pulse intervals before and after
274 stimulation (18.33 ± 1.18 min vs. 17.08 ± 1.25 min, $n = 4$, $p > 0.05$; Fig. 5**C**&**D**).

275 **Selective optogenetic stimulation of UCN3-expressing GABA neurons fails to affect pulsatile**
276 **LH secretion in female mice.**

277 To further test the functional interactions between the UCN3 and GABAergic populations, a
278 separate cohort of UCN3-Cre::VGAT-Flpo transgenic female mice was injected with an AAV-nEF-
279 Con/Fon 2.0-ChRmine-oScarlet viral construct, which allows optogenetic stimulation of UCN3
280 neurons co-expressing GABA (UCN3-expressing GABA) (Con/Fon group). Statistical analysis
281 showed no significant interaction effect of group and optogenetic stimulation on LH inter-pulse
282 intervals (two-way ANOVA, $F(1, 14) = 0.4306$, $p = 0.5223$). That is, LH inter-pulse intervals in the
283 Con/Fon group, showed no change following optogenetic stimulation compared to the control period
284 (17.92 ± 0.80 min vs. 16.60 ± 0.88 min, mean ± SEM, $n = 6$, $p > 0.05$; Fig. 5**H**&**J**). Similarly, in the
285 no-stimulation control experiment for this cohort, which did not receive optogenetic stimulation, there
286 was no significant difference in LH inter-pulse intervals (15.42 ± 2.53 min vs. 15.83 ± 1.67 min, $n =$
287 3, $p > 0.05$; Fig. 5**I**&**J**).

288 Taken together, our results suggest that UNC3 and GABAergic populations are functionally
289 orthogonal in the MePD circuit, i.e., activation of UCN3 neurons relay inhibitory information to the
290 hypothalamic GnRH pulse generator but activation of the UCN3 neurons that co-expressing GABA
291 are not sufficient.

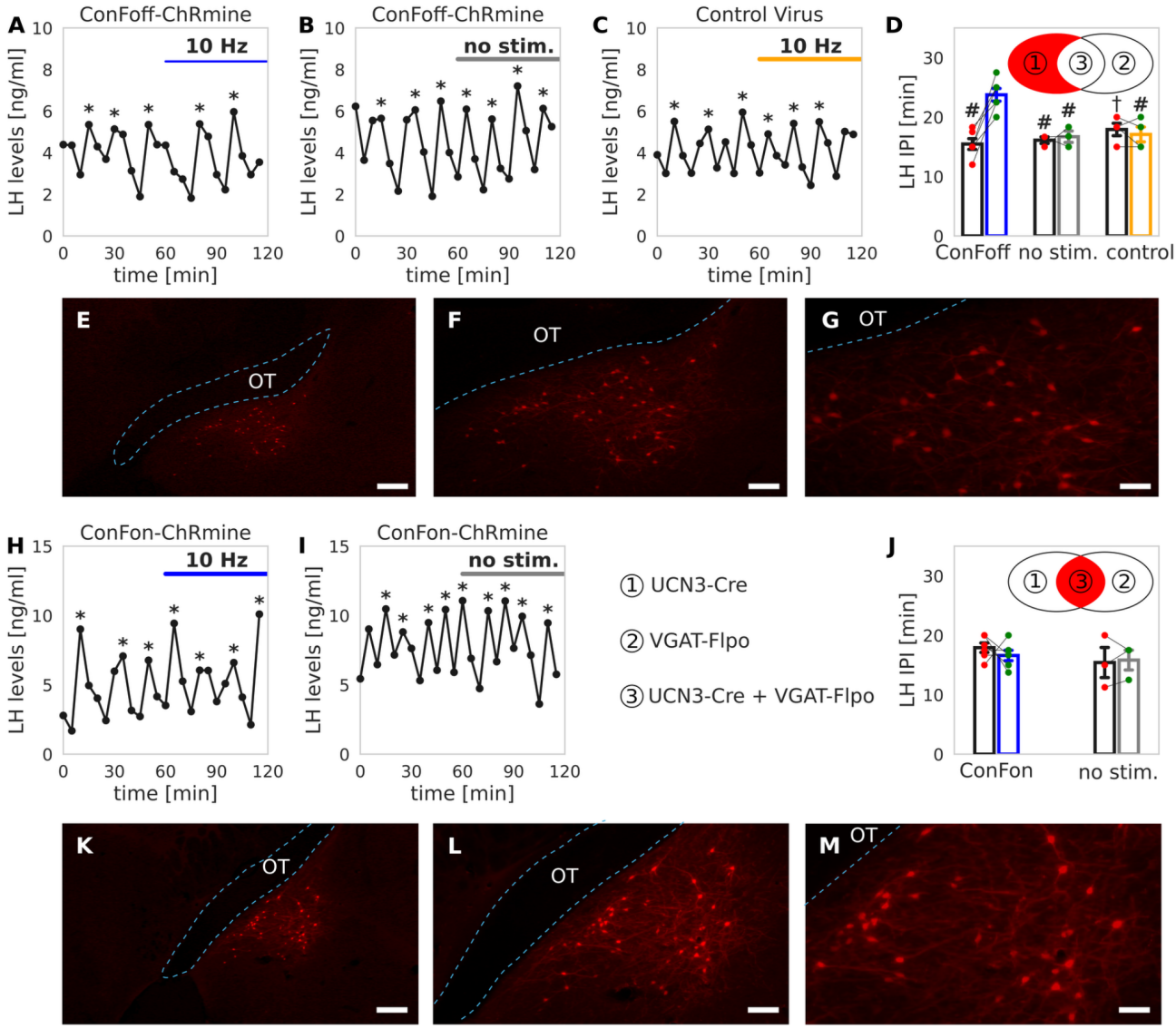

292

293 **Figure 5: Effect of optogenetic stimulation of UCN3 non-GABAergic and UCN3 neurons co-expressing**
294 **GABA in the MePD on LH pulse frequency.** (**A**-**D**) Optogenetic stimulation of UCN3 non-GABAergic
295 neurons inhibited LH pulses. Representative examples of LH pulsatility in UCN3-Cre::VGAT-Flpo mice
296 injected with AAV-Con/Foff-ChRmine in response to (**A**) 10Hz optic stimulation or (**B**) no stimulation as
297 control, and (**C**) in mice injected with control virus in response to 10 Hz stimulation. Pulses detected by the
298 DynPeak algorithm are indicated with an asterisk (*). (**D**) Mean LH inter-pulse interval (IPI) (±SEM) for each
299 group during the control period and over the subsequent stimulation period. #: $p<0.01$ vs stimulation period in
300 Con/Foff group (Two-way ANOVA, Tukey's post-hoc). (**E**-**G**) Representative photomicrographs of expression
301 of AAV-nEF-Con/Foff 2.0-ChRmine-oScarlet (red) in MePD UCN3 neurons. (**H**-**M**) Optogenetic stimulation of
302 neurons co-expressing UCN3 and GABA in the MePD did not impact LH pulse significantly. Representative

303 examples of LH pulsatility in UCN3-Cre::VGAT-Flpo mice injected with Con/Fon-ChRmine-oScarlet virus in
304 response to (**H**) 10 Hz optic stimulation or (**I**) no stimulation as control. (**J**) Mean LH IPI (±SEM) for each group
305 during the control period and over the subsequent stimulation period (Two-way ANOVA). (**K**-**M**)
306 Representative photomicrographs of neurons co-expression UCN3 and GABA, tagged with oScarlet (red).
307 Scale bars represent (**E**&**K**) 200 μm, (**F**&**L**) 100 μm, (**G**&**M**) 50 μm. OT, optic track.

308 **The MePD GABAergic neurons relay information from UCN3 neurons and inhibit the GnRH**
309 **pulse generator.**

310 To test our remaining model predictions and establish the functional role of GABAergic neurons in
311 the MePD in transmitting inhibitory signals to the hypothalamic GnRH pulse generator, we injected
312 the AAV-EF1a-ChR2 viral construct into VGAT-Cre transgenic mice, targeting the entire MePD
313 GABA neuron population for expressing ChR2 and used the optogenetic stimulation protocol
314 described above (60 min control period followed by 60 min stimulation) to stimulate the entire MePD
315 GABAergic population. Statistical analysis showed a significant interaction effect of our genetic
316 intervention and stimulation period on LH pulsatility ($F_{(2,18)} = 7.567$, $p = 0.0041$; two-way ANOVA).
317 Stimulation of the GABAergic population markedly increased the LH inter-pulse interval compared to
318 the pre-stimulation control period (18.5 ± 2.03 min vs 49.5 ± 8.46 min, mean ± SEM, n = 5, $p<0.01$;
319 Tukey's post-hoc; Fig. 6**A**&**D**), validating modeling prediction 2. In contrast, mice that did not receive
320 optogenetic stimulation showed no change in LH inter-pulse interval (23.13 ± 4.25 min vs 20.00 ±
321 1.77 min, n = 4, $p > 0.05$; Tukey's post-hoc; Fig. 6**B**&**D**). Similarly, control virus (AAV-EF1a-DIO-
322 EYFP) injections did not result in any significant difference in LH inter-pulse interval before and
323 during stimulation (15.83 ± 0.83 min vs 18.33 ± 0.96 min, n = 3, $p > 0.05$; Tukey's post-hoc; Fig.
324 6**C**&**D**).

325 Next, UCN3-Cre::VGAT-Flpo transgenic females were injected with an intersectional viral mixture
326 containing AAV-nEF-Con/Foff 2.0-ChRmine-oScarlet and pAAV-nEF-Coff/Fon-NpHR3.3-EYFP ,
327 enabling simultaneous excitation of UCN3 non-GABA neurons and inhibition of non-UCN3
328 GABAergic neurons. Statistical analysis showed no significant interaction effect of genetic
329 manipulation and stimulation period on LH pulsatility ($F_{(1, 14)} = 0.2338$, $p = 0.6362$; two-way ANOVA).

330 Moreover, optogenetic stimulation resulted in no significant change in the LH inter-pulse interval
331 relative to the control period (16.67 ± 1.31 min vs 18.61 ± 1.58 min, mean ± SEM, n = 6, $p > 0.05$;
332 Fig. 6**H**&**J**), which aligns with our modeling prediction 3. Similarly, in mice injected with the same
333 viral mixture but without receiving optogenetic stimulation, no significant change in LH inter-pulse
334 interval was detected (16.39 ± 2.47 min vs 16.67 ± 0.83 min, n = 3, $p > 0.05$; Fig. 6**I**&**J**).

335 Collectively, these findings suggest that MePD GABAergic neurons are integral to regulating LH
336 pulse frequency. The inhibitory effect on LH pulses observed upon UCN3 neuron activation is
337 attenuated when GABAergic neuron activity is optogenetically suppressed, implying that GABAergic
338 signaling acts downstream of UCN3 neurons, relaying the inhibitory signal to the hypothalamic
339 GnRH pulse generator.

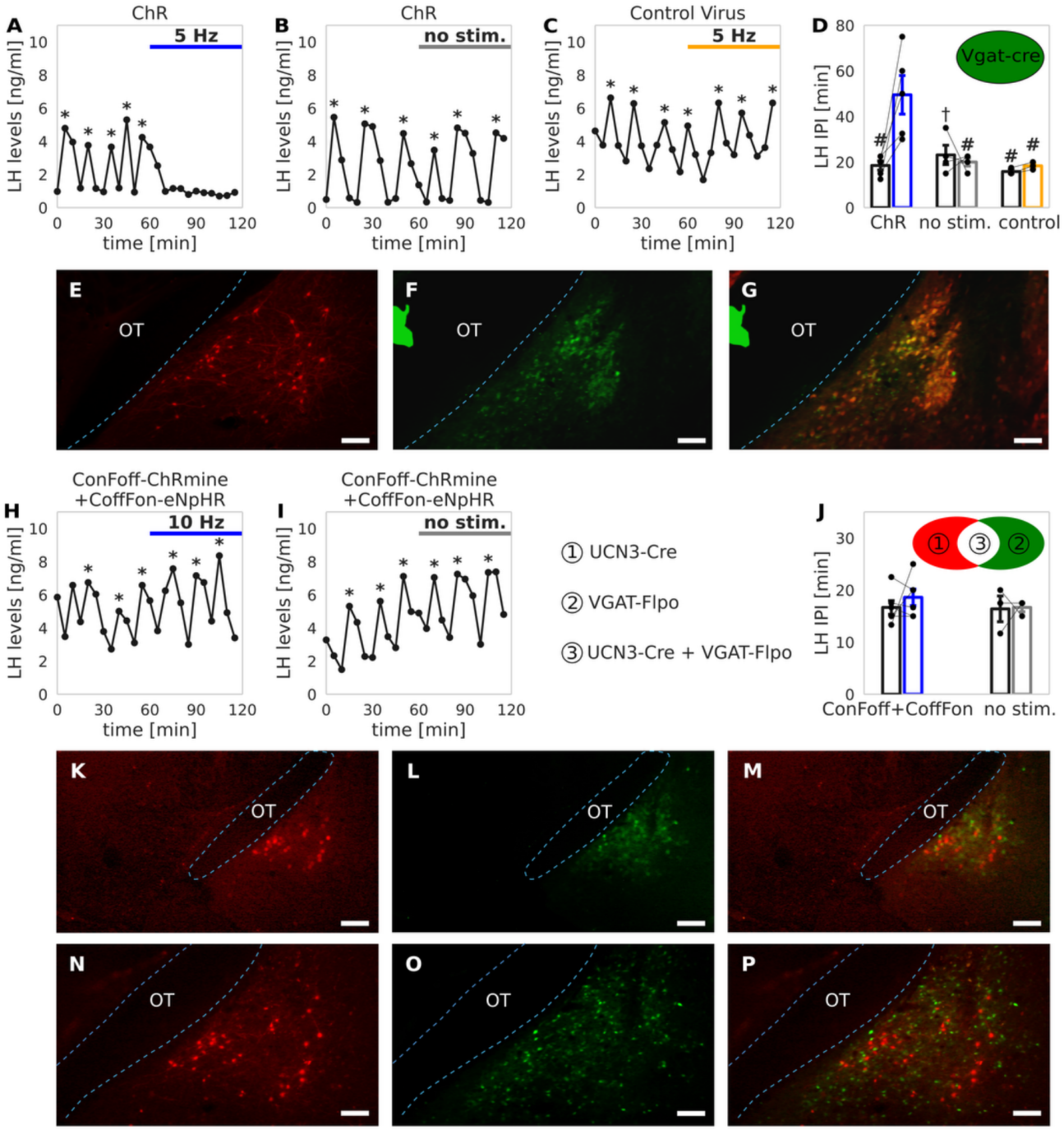

Figure 6: Selective optogenetic stimulation of GABA neurons in the MePD inhibits LH pulsatility and their activity is necessary for mediating UCN3 signalling downstream. (**A-G**) Optogenetic activation of the entire MePD GABA population in VGAT-Cre mice led to significant LH pulse suppression. Representative examples showing LH pulsatility in VGAT-Cre mice injected with AAV-double floxed-ChR2-EYFP virus in response to (**A**) 5 Hz stimulation or (**B**) no stimulation as control, and (**C**) 5 Hz stimulation in mice injected with control virus. (**D**) Mean LH IPI (±SEM) for each group during the control period and over the subsequent

347 stimulation period. #: p<0.01, †: p<0.05 vs stimulation period in ChR group (Two-way ANOVA, Tukey's post-
348 hoc). (**E-G**) Representative photomicrographs of MePD GABA neurons, labeled with (**E**) tdTomato (red), (**F**)
349 ChR2-EYFP (green), and (**G**) merged. Scale bars represent. (**H-P**) The simultaneous inhibition of non-UCN3
350 GABA neurons in the MePD restored the LH suppression induced by stimulation of non-GABAergic UCN3
351 neurons. Representative examples showing LH pulsatility in UCN3-Cre::VGAT-Flpo female mice injected with
352 Con/Foff-ChRmine-oScarlet and Coff/Fon-NpHR-EYFP virus mixture in response to (**H**) 10 Hz optogenetic
353 stimulation or (**I**) no stimulation as control. (**J**) Mean LH IPI (±SEM) for each group during the control period
354 and over the subsequent stimulation period. (Two-way ANOVA). (**K-P**) Representative photomicrographs of
355 fluorescence in MePD neurons. (**K**&**N**) non-GABAergic UCN3 neurons tagged with oScarlet (red), (**L**&**O**) non-
356 UCN GABA neurons tagged with EYFP (green) (**M**&**P**) merged. Scale bars represent (**E-G**) 150 µm, (**K-M**)
357 200 µm, (**N-P**) 100 µm.

358 ## Discussion

359 The posterodorsal subnucleus of the Medial Amygdala (MePD), is a critical regulator of reproductive
360 function. Single-cell transcriptomics has revealed a mosaic of glutamatergic and GABAergic
361 populations in this region, with GABA neurons co-expressing receptors for gonadal steroids as well
362 as neuromodulators and cognate receptors involved in parental and sociosexual behavior (including
363 kisppeptin, prolactin and oxytocin)[19]. Furthermore, calcium imaging of neuronal ensembles from this
364 region have started to decipher how this brain region encodes information about social interactions
365 and stressful stimuli[20], with stress related information being relayed to the reproductive axis via
366 potentially direct projections to the hypothalamus[1,2], and eliciting well-documented responses on
367 pubertal timing[6,7], LH secretion[10,11] and the GnRH pulse generator[3–5]. Here, to elucidate the
368 neuronal circuitry involved in MePD processing of stress signals, we used GRIN lens mini-
369 endoscopic calcium imaging to study, for the first time, the dynamic activity of MePD GABAergic and
370 UCN3 neurons under acute restraint stress as well as the activity of GABAergic neurons in response
371 to UCN3 activation. Functional network analysis of the imaging data revealed that acute restraint
372 stress induces a functional reconfiguration of the GABAergic population, emphasizing the pivotal
373 role of GABA neurons in encoding and transmitting stress information. A comparable reconfiguration

374 was observed following optogenetic stimulation of UCN3 neurons, suggesting that these two
375 populations are co-involved in stress processing. Further clustering analysis of the calcium
376 transients identified two distinct GABAergic sub-populations with anti-correlated activity. This finding
377 of two distinct populations is consistent with physiological and morphological studies of GABAergic
378 neurons in the medial amygdala characterizing them as either projecting cells or interneurons[12,14].

379 Building upon our previously developed computational model of the MePD circuit, we explored the
380 neuronal pathways underlying stress processing. The model consists of a glutamatergic sub-
381 population and two GABAergic sub-populations: one comprising GABAergic interneurons and the
382 other GABAergic efferent neurons. Our analysis identified two conditions necessary for the anti-
383 correlated activity between these GABAergic sub-populations, consistent with our experimental
384 observations. First, mutual inhibition between the GABA sub-populations is required, where
385 activation of one sub-population suppresses the activity of the other. Second, if both sub-
386 populations receive a shared input (e.g., from the glutamatergic population or in fact any other
387 population of excitatory cells), their dynamics become entrained to that common stimulus, meaning
388 that distinct input streams to each sub-population are necessary for the observed anti-correlation.
389 To satisfy this condition in our model, GABAergic interneurons receive inputs from UCN3 neurons,
390 whereas the GABAergic efferent sub-population receives inputs from glutamatergic neurons. This
391 circuitry implies that stress information is processed along two key pathways (one glutamatergic and
392 one GABAergic) and is integrated by the GABAergic efferent neurons.

393 We note that an alternative connectivity pattern, with the UCN3 population directly projecting to the
394 GABA efferent population, could also fit our experimental observations, but does not reproduce
395 previously published results on the effects of neuropharmacological perturbations in the MePD on
396 LH pulsatility[17]. Specifically, the suppression of glutamatergic neurons in combination with
397 stimulation of UCN3 neurons. Under this scenario direct input from stimulated UCN3 to GABA
398 efferent neurons will lead to the increase in its activity, consequently increasing KNDy IPI. This
399 finding contrasts with experimental observations, where the combined suppression of glutamate and
400 stimulation of UCN3 failed to produce any significant change in GnRH pulsatility[17].

401 Consistent with model predictions, we showed that optogenetic activation of UCN3-expressing non-
402 GABAergic neurons suppresses LH pulse frequency. This finding corroborates previous work
403 demonstrating that LH pulses are inhibited by activation of UCN3 neurons[7,17] or administration of
404 UCN3[10] in the MePD, and that such effects are attenuated by chemogenetic inhibition of UCN3
405 neurons or by antagonizing corticotropin-releasing factor type 2 receptors (CRFR2)[10]. Thus, our
406 findings further support the central role of UCN3 signaling in modulating both stress responses and
407 reproductive function.

408 GABA is one of the primary inhibitory neurotransmitters in the nervous system[12]. Previous work has
409 shown that GABAergic neurons in the MePD project to the ARC to regulate LH pulses and
410 chemogenetic inhibition of MePD GABA neurons attenuates stress-induced suppression of LH
411 pulses[11]. In this study, we found that optogenetic activation of GABAergic neurons in the MePD
412 leads to robust LH pulse suppression, reinforcing the pivotal role of GABAergic signaling in stress-
413 related reproductive dysfunction. Antagonizing GABA receptors in the MePD can block UCN3-
414 induced LH suppression[17], suggesting that GABAergic neurons function downstream of UCN3
415 signaling. However, this pharmacological approach lacks cell-type specificity, leaving open the
416 possibility that UCN3 neurons themselves co-expressing GABA receptors, potentially contributing to
417 the observed effect. Here, by using an intersectional genetic strategy, we demonstrated that
418 optogenetically inhibiting non-UCN3 GABAergic neurons can abolish the change in LH pulse
419 intervals induced by optogenetic stimulation of UCN3 neurons. This finding provides evidence that
420 these GABAergic neurons act downstream of UCN3 signaling to mediating LH pulse suppression.
421 We note, that while in our current experimental protocol we could also be blocking GABAergic
422 projections to the ARC KNDy population, which by itself could explain the absence of any effect
423 from UCN3 stimulation, our modeling predicts that GABAergic interactions within the MePD are
424 additionally crucial for relaying UCN3 signals to the KNDy network as also suggested by
425 pharmacologically antagonizing GABA receptors[17].

426 It is not unusual for neurons to co-express neuropeptides and neurotransmitters[14]. Given that
427 activating either UCN3 or GABAergic neurons independently suppresses LH pulses, one might

428 predict that stimulating neurons co-expressing both UCN3 and GABA would similarly inhibit LH.
429 However, we observed no significant changes in LH pulses upon optogenetic stimulation of neurons
430 co-expressing UCN3 and GABA. This suggests the two populations are functionally orthogonal:
431 although both UCN3 and GABA neurons are essential for LH pulse inhibition, their overlap is not.
432 Within our modeling framework, UCN3/GABA co-expressing neurons might be considered part of
433 the GABAergic interneuron population, primarily inhibiting GABA projection neurons rather than
434 activating them. Consequently, they fail to relay the inhibitory UCN3 signal to the ARC. Further
435 studies are necessary to define more precisely the distinct role of UCN3/GABA neurons within the
436 MePD circuitry.

437 By combining mini-endoscopic calcium imaging with computational modeling, we identified two
438 GABAergic sub-populations with complementary but distinct roles in encoding stress signals and
439 modulating LH pulsatility. Our experimental and computational results also stressed the functional
440 orthogonality between UCN3 and GABA signaling in MePD, highlighting the complexity of the
441 MePD's contribution to stress-induced reproductive suppression. These results offer valuable
442 insights into the neuronal circuits potentially involved in processing stress-related effects in
443 reproduction, paving the way for future research aimed at improving reproductive health and well-
444 being.

445 # Methods

446 **Animal**

447 VGAT-Cre-tdTomato mice were genotyped using PCR to determine heterozygosity for VGAT-Cre
448 (primers 5′-3′: common, 12785—CTTCGTCATCGGCGGCATCTG; wild-type reverse12786—
449 CAGGGCGATGTGGAATAGAAA; mutant reverse oIMR8292—CCAAAAGACGGCAATATGGT) and
450 tdtomato (primers 5′-3′: wild-type forward oIMR9020—AAGGGAGCTGCAGTGGAGTA; wild-type
451 reverse oIMR9021—CCGAAAATCTGTGGGAAGTC; mutant reverse WPRE oIMR9103—
452 GGCATTAAAGCAGCGTATCC; mutant forward tdTomato oIMR9105—
453 CTGTTCCTGTACGGCATGG). UCN3-Cre heterozygous mice (strain Tg(Ucn3-cre)KF43Gsat/

454 Mmucd, MMRRC GENSAT) were crossbred with VGAT-Flpo heterozygous mice (Jax stock
455 #007909,B6.Cg-Slc32a1 2A-Flpo-D:Het) to obtain female double heterozygous UCN3-Cre::VGAT-
456 Flpo mice (Slc32a1 2A-Flpo-D:Het|Ucn3-Cre:Het|Rosa26<tomato>WT); genotyped using PCR for
457 the detection of heterozygosity (primers 5′- 3′: UCN3 Forward: CGAAGTCCCTCTCACACCTGGTT;
458 Cre Reverse: CGGCAAACGGAC-AGAAGCATT; Slc32a1 Mutant Forward: TGC ATC GCA TTG
459 TCT GAG TAG; Slc32a1 Mutant Reverse: GAC AGC CGT GAA CAG AAG G). Female mice, aged 8
460 to 10 weeks, weighing between 20 g and 25 g, were individually housed in ventilated cages sealed
461 with a HEPA-filter at 25 ± 1°C in a 12:12-hour light/dark cycle, lights on at 07:00 h. Vaginal smears
462 were performed when mice are 6 weeks old between 10:00 - 12:00 h daily. Only mice showing
463 regular estrous cycles were included. All animal procedures performed were approved by the King's
464 College London Animal Welfare and Ethical Review Body. Procedures were in accordance with UK
465 home office regulation.

466 **Stereotaxic injection of adeno-associated virus construct and fiber-optic or mini-endoscope**
467 **GRIN lens implantation**

468 All surgical procedures were carried out under general anaesthesia using ketamine (Vetalar, 100
469 mg/kg, i.p.; Pfizer, Sandwich, UK) and xylazine (Rompun, 10 mg/kg, i.p.; Bayer, Leverkusen,
470 Germany) under aseptic conditions. Animals were secured in a David Kopf stereotaxic frame (Model
471 900, Kopf Instruments, CA, USA). Following bilateral ovariectomy, a midline incision was made in
472 the scalp to reveal the skull. Two small bone screws were inserted into the skull. A small hole was
473 drilled above the position of the MePD. The MePD coordinate (2.29 mm lateral, 1.60 mm posterior
474 from bregma, at a depth of 5.33 mm below the skull surface) was determined according to the
475 mouse brain atlas of Paxinos and Franklin[21]. A unilateral stereotaxic viral injection was performed to
476 target opsin or fluorescent protein expression in the MePD neurons, using a robot stereotaxic
477 system (Neurostar, Tubingen, Germany), with a 5-μL Hamilton microsyringe (Esslab, Essex, UK), at
478 the speed of 25 nl/min for 10 min.

479 Two transgenic animal models were used for LH blood sampling under optogenetic stimulation:
480 UCN3-Cre::VGAT-Flpo and VGAT-Cre-tdTomato. The following types of viral constructs were used
481 in separated cohorts of UCN3-Cre::VGAT-Flpo mice: (i) AAV-nEF-Con/Foff 2.0-ChRmine-oScarlet
482 (250 nl, 2.1×10^{12} gc/mL, Serotype:8, #137161, Addgene, Massachusetts, USA); (ii) AAV-nEF-
483 Con/Fon 2.0-ChRmine-oScarlet (250 nl, 1.9×10^{12} gc/mL, Serotype:8, # 137159, Addgene,
484 Massachusetts, USA); (iii) a mixture of AAV-nEF-Con/Foff 2.0-ChRmine-oScarlet (2.1×10^{12} gc/mL,
485 #137161) and pAAV-nEF-Coff/Fon-NpHR3.3-EYFP (1.9×10^{12} gc/mL; #137159, final volume 300 nl);
486 (iv) control virus AAV-Ef1a-DIO-EYFP (250 nl, 4.4×10^{12} gc/mL, Serotype:9, #27056, Addgene,
487 Massachusetts, USA). VGAT-Cre-tdTomato mice received unilateral injections of (i)
488 channelrhodopsin (ChR2) viral construct, (250 nl, 1.8×10^{12} gc/mL; Serotype:9; Addgene, #20298,
489 Massachusetts, USA) or (ii) control virus, AAV-Ef1a-DIO-EYFP (250 nl, 4.4×10^{12} gc/mL,
490 Serotype:9; Addgene, # 27056, Massachusetts, USA) into the MePD. Following injection, the needle
491 was kept in position for 10 min before going up slowly over 1 min. A unilateral fibre optic cannula
492 (200 μm, 0.39 NA, 1.25 mm ceramic ferrule; Doric Lenses, Quebec, Canada) was inserted into the
493 right MePD 0.15 mm above the injection site. After reaching the target, the fibre optic cannula was
494 secured on the skull using dental cement (Super-Bond Universal Kit, Prestige Dental, UK), bonded
495 to the screws and skull. Finally, the incision in the scalp was closed with suture. Animals were given
496 1 week to recover, after which they were handled 20 min daily to acclimatize to experimental
497 procedures for a further 2 weeks.

498 For mini-endoscope *in vivo* calcium imaging, only UCN3-Cre::VGAT-Flpo transgenic animals were
499 used. Separate mice cohorts received the following viral injection into the MePD: (i) a mixture of
500 pAAV-Syn-Flex-rc[Chrimson-tdTomato] (2.0×10^{12} gc/mL, Serotype:5, #62723, Addgene,
501 Massachusetts, USA) + pAAV-EF1a-fDIO-GCaMP6s (2.3×10^{12} gc/mL; Serotype:8; #105715,
502 Addgene, Massachusetts, USA; final volume 400 nl); (ii) a mixture of pAAV-Syn-Flex-rc[Chrimson-
503 tdTomato] (2.0×10^{12} gc/mL, Serotype:5, #62723, Addgene, Massachusetts, USA) +
504 pAAV.CAG.Flex.GCaMP6s.WPRE.SV40 (4.3×10^{12} gc/mL; Serotype:9; # 100842, Addgene,
505 Massachusetts, USA; final volume 400 nl); (iii) a mixture of control virus AAV-Ef1a-DIO-EYFP (250

506 nl, 4.4×10^{12} gc/mL, Serotype:9, #27056, Addgene, Massachusetts, USA) + pAAV-EF1a-fDIO-
507 GCaMP6s (2.3×10^{12} gc/mL; Serotype:8; #105715, Addgene, Massachusetts, USA; final volume 250
508 nl). One week after administering the virus, a 600-µm diameter, 7.2-mm long gradient index (GRIN)
509 ProView™ Integrated Lens (Inscopix, PN:100-004554) was implanted at the same location as the
510 viral injection. The surface of the skull was scored, using the tip of a surgical scalpel, and four
511 screws were inserted into the skull. This was done to enhance the adhesion of dental cement to the
512 skull, thereby reducing the interference of movement on *in vivo* recording. Before insertion of the
513 GRIN lens, a 23 G needle was slowly lowered at a speed of 5.0 mm/min into the brain (2.42 mm
514 lateral, 1.52 mm posterior from bregma, depth of 5.05 mm below the skull surface) to make a needle
515 track to facilitate the insertion of the GRIN lens without causing brain distortion along its route. The
516 GRIN lens was then inserted into the brain at a rate of 0.6 mm/min, using the same coordinates as
517 the needle precutting. To secure the GRIN lens with integrated baseplate in position, we used a light
518 curing adhesive (iBond Universal, Kulzer GmbH, Leipziger, Germany) along with a cured
519 radiopaque hybrid dental cement (Gradia Direct Flo, GC corporation, Tokyo, Japan), bonding it to
520 the head screws and skull. A GRIN lens baseplate dust cover (Inscopix) was rescued in place to
521 protect the lens. After 4 weeks the mice were re-anaesthetized as described above and underwent
522 bilateral ovariectomy.

523 **Serial blood sampling for LH measurement**

524 The mouse's tail-tip was excised using a sterile scalpel. Then the chronically unilaterally implanted
525 fibre optic cannula was connected to a multimode fibre optic rotary joint patch cables (Thorlabs Ltd,
526 Ely, UK) via a ceramic mating sleeve to allow the animal freedom of movement. Mice were left for 1
527 h to habituate. A Grass SD9B stimulator-controlled DPSS laser (Laserglow Technologies, Toronto,
528 Canada) was utilised to deliver either green light (532 nm wavelength, 10 Hz, 5 seconds on 5
529 seconds off, 10 mW, 10-ms pulse width,) or blue light (473 nm wavelength, 5 Hz, 5 seconds on 5
530 seconds off, 5 mW, 10-ms pulse width,). The light pattern was controlled using software designed in
531 house. After 1 h of acclimatization, serial blood samples (5-µL) for LH pulse measurement were
532 collected every 5 min for 2 h between 10:00 - 12:00 h: 0-60 min for control blood sampling period,
533 and 60-120 min under stimulation or equivalent no-stimulation control period. Blood samples were

534 diluted in 45 μL of 0.2% BSA-0.05% PBS with Tween-20 (0.2% BSA and 0.05% PBST) and

535 immediately placed on dry ice and stored at −80°C until later analysis.

536 **LH assay**

537 LH measurement was performed using an LH ELISA assay as reported previously[22]. A mouse LH
538 standard (mLH; AFP-5306A, NIDDK-NHPP, USA) was used to establish a standard curve for the
539 quantitative measurement. The following antibodies were used in the assay: (i) coating antibody
540 (RRID: AB_2665514, monoclonal antibovine LH beta subunit antiserum, 518B7, University of
541 California, CA, USA); (ii) anti-LH antibody (RRID: AB_2665533; National Hormone & Peptide
542 Program, CA, USA); (iii) secondary antibody (RRID: AB_772206, GE Healthcare, Chicago, Illinois,
543 USA). The inter-assay and intra-assay variations were 10.53% and 5.74%, respectively. The assay
544 sensitivity was 0.023 ng/mL.

545 **LH pulse statistical analysis**

546 LH pulses were verified using the Dynpeak algorithm in Scilab 5.5.2 programme[23]. The Dynpeak
547 algorithms were classified for OVX mice based on previously established parameters[24]. The average
548 LH inter-pulse interval was calculated for the 1-h control period and the 1-h stimulation period in both
549 experimental and control mice. Statistical significance was assessed using a 2-way ANOVA unless
550 otherwise stated. Data was represented as mean ± SEM and $p<0.05$ was considered significant.

551 **Mini-endoscope-based Calcium imaging**

552 **Under optogenetic stimulation of MePD UCN3 neurons.** Prior to recording, animals were
553 handled daily for 5 to 6 weeks to get accustomed to the experimental setup. The Data Acquisition
554 (DAQ) box (Inscopix, PN:100-005904) was turned on and connected to the computer wirelessly.
555 The Data Acquisition Software (IDAS; Inscopix, Inc.) was accessed through the Chrome web
556 browser on the computer communicating with the DAQ box. Adequate DAQ box storage capacity
557 was checked routinely before Calcium imaging. The GRIN lens baseplate dust cover was gently

558 removed from the mouse's head, after which the minscope camera was secured to the baseplate
559 platform. Equipped with the head-mount miniscope (nVoke2, Inscopix, SN: BB-11238601), the
560 mouse was then placed back into its home cage. The optimal focal plane was chosen by adjusting
561 the lens focus to achieve clear cell morphology. The exposure time was fixed at 50 ms. The frame
562 rate was set to 20 Hz. Subsequently, gain, and LED power were optimized based on image
563 histograms before initiating recording. Two types of LED were used during the recording: (i) EX-LED
564 (0.2-0.4 mW, 435-460 nm excitation filter) for GCaMP6s signal detection in the GABAergic or UCN3
565 neurons; (ii) OG-LED (10 mW, 590-650 nm excitation filter) for Chrimson optogenetic stimulation of
566 the UCN3 neurons. After the mice were attached to the miniscope, they were given 1-2 h for
567 adaptation. For stimulation of the UCN3 neurons, the OG-LED was set to 10 Hz, 5 seconds on 5
568 seconds off, and a 10-ms pulse width. Once the animals had acclimatized, the GCaMP6s recording
569 of the GABAergic neurons or UCN3 neurons was started with a protocol of 2 min baseline before
570 stimulation for 2 min. Optogenetic stimulation was randomized for the 10 Hz, with a 5-min interval
571 between each to prevent photobleaching of GCaMP6s. Once the experiment was concluded, the
572 miniscope was gently detached, and the baseplate cover was reattached and secured with its
573 screw. The recordings were performed between 9:00 h and 15:00 h. Three groups of animals were
574 included in this experiment: (i) mice with UCN3 neurons expressing opsin and GABAergic neurons
575 expressing GCaMP; (ii) mice with UCN3 neurons expressing both opsin and GCaMP, serving as a
576 positive control; (iii) mice with UCN3 neurons expressing mCherry and GABAergic neurons
577 expressing GCaMP, serving as a negative control.

578 **Under restraint stress.** The system was set up and the mouse was connected to the miniscope as
579 described above but with the OG-LED turned off. Once the mouse had settled, the experiment
580 started with a 3 min baseline recording, followed by 3 min of recording under hand-held restraint.
581 Finally, the miniscope was detached and the baseplate cover was reattached. The experiments were
582 performed between 9:00 h and 15:00 h. The animals in this experiment were the same as those
583 used in the optogenetic stimulation protocol described above, but were divided into two groups

584 depending on whether GCaMP was expressed in the UCN3 or GABAergic neurons, regardless of
585 whether opsin or mCherry was expressed in the UCN3 cells.

586 ***In vivo* calcium imaging recording processing**

587 The video data, with a resolution of 1280 pixels x 800 pixels, was exported from the DAQ box
588 through the file manager to a desktop computer and processed with the Inscopix Data Processing
589 Software (IDPS). Within the IDPS, there are six essential steps for extracting single-cell calcium
590 transient data from the recorded video: down-sampling, cropping, spatial filtering, motion correction,
591 trace normalization (ΔF/F), and cell identification. First, the video underwent both spatial down-
592 sampling and temporal down-sampling by a factor of 2 and was cropped to enhance processing
593 speed, focusing on the region of interest where the GCaMP signal was observed. Spatial filtering,
594 with a threshold ranging between 0.005 (low) and 0.5 (high) was used to distinguish individual pixels
595 in the video image, creating a high-contrast image. A mean intensity projection image was
596 generated. Motion correction was subsequently conducted, using the mean intensity projection
597 image as a reference. Motion correction was applied again using one of the frames affected by
598 movement while simultaneously drawing a region of interest (ROI) where UCN3 accumulates to
599 enhance the effectiveness of motion correction. For the recordings with GCaMP signals from
600 GABAergic neurons, we did not use the built-in motion correction function of IDPS. Instead, we used
601 the MATLAB (version R2022a) implementation of the open-source algorithm NoRMCorre[25] with
602 default parameters for both rigid and non-rigid (patch size 64 pixels and overlap 32) motion
603 correction as long as a minimum correlation of the frames with the mean frame above 0.8 is
604 achieved. Occasionally, if the minimum correlation is not met, an extra step of non-rigid motion
605 correction with coarser patches is applied. This is performed by doubling the patch size and their
606 overlap to 128 and 64, respectively. Corrected videos were saved in TIFF format for further analysis
607 via IDPS. Following motion correction, pixel intensity, $F(x,y)$, in each frame of the movie was
608 normalised using the following formula $\frac{(F(x,y) - F_{baseline}(x,y))}{F_{baseline}(x,y)}$, where $F_{baseline}(x,y)$ is the baseline
609 pixel intensity calculated by taking the mean value of the pixel across the entire movie. Finally,

610 regions of interest were identified automatically using the cell identification algorithm provided by
611 IDPS, based on principal component and independent component analysis (PCA-ICA algorithm).

612 **Validation of virus injection, fibre optic cannula and GRIN lens implantation**

613 Once the experimental procedures were completed, a lethal dose of ketamine was used to
614 humanely euthanize the mice. The mice were perfused transcardially with heparinised saline (5
615 U/ml) for 5 min, followed by ice-cold 4% paraformaldehyde (PFA) for 15 min using a pump
616 (Minipuls,156 Gilson, Villiers Le Bel, France). The brains were collected and post-fixed sequentially
617 at 4°C in a solution of 15% sucrose in 4% PFA and later in a solution of 30% sucrose in phosphate
618 buffer until they sank. They were then snap frozen on dry ice and stored in -80°C until processing.
619 The brains were coronally sectioned (30 μm) between +0.5 mm and -2.7 mm from the bregma using
620 a cryostat (Bright Instrument Co., Huntingdon, UK), and sections were mounted on microscope
621 slides, air-dried, and covered with slips using Prolonged Antifade mounting medium (Molecular
622 Probes, Inc. OR, USA). The accuracy of injection sites, fibre optic cannula and GRIN lens
623 implantation were confirmed by Axioskop 2 Plus microscope equipped with AXIOVISION 4.7
624 (Zeiss). Images were captured using Axioskop 2 Plus microscope (Carl Zeiss). Only the data of
625 mice with correct viral infection and implantation of cannula and lens in the MePD were included in
626 the analysis.

627 **Data analysis**

628 The data processing protocol we employ in this study was performed in two phases: pre-intervention
629 and intervention (either via optogenetic stimulation or restraint stress). For our analysis, we use the
630 smoothed deconvolved traces generated by the OASIS method[26], which improves the signal-to-
631 noise ratio (SNR) and mitigates noise interference. All traces are rescaled between 0 and 1 (min-
632 max normalization), and then further normalized to mean zero and unit variance. The analysis
633 process is divided into three key steps: i) identification of GABA cells co-expressing UCN3 and
634 removing them from further analysis; ii) estimating and comparing functional connectivity before and
635 during intervention; iii) clustering analysis based on pairwise association-derived dissimilarity scores.

636 In step (i), we use power spectral density (PSD) analysis and K-means clustering (using Euclidean
637 distance) to identify GABA neurons with activity that mimics the pattern of optic stimulation, evidence
638 that they are co-expressing UCN3.

639 **PSD filtering.** For each trace, we compute the PSD during the stimulation phase. Cells with PSD
640 values at 0.1 Hz (the frequency of the stimulus 5 seconds on and 5 seconds off cycle) above 0.37
641 Hz^{-1} are labelled as co-expressing UCN3. This threshold is determined from recordings of UCN3
642 cells under optic stimulation, by calculating the median of the minimum PSD values at 0.1 Hz from
643 each dataset (see Supplementary Fig. 8 **B**).

644 **K-means clustering.** Using the Euclidean distance metric, we cluster the traces during the
645 stimulation phase into two groups, aiming to separate neurons into GABA-only neurons and neurons
646 co-expressing UCN3 and GABA. Clustering separated a small group of neurons with activity
647 mimicking the optic stimulation oscillatory pattern (see Supplementary Fig. 8 **C**). Recordings of
648 MePD UCN3 neurons shows that under optogenetic stimulation their activity rises and declines in
649 phase with on and off periods of stimulation (shown in Fig. 3**A**); therefore, this small number of cells
650 was labelled as co-expressing UCN3.

651 The union of neurons identified by either method as co-expressing UCN3 and GABA are excluded
652 from further analysis. By applying both filters, we aim to robustly identify purely GABA-expressing
653 neurons. We acknowledge the possibility that some cells may pass through the filters or that a few
654 purely GABA-expressing neurons may be inadvertently excluded. However, our dual approach of
655 employing power spectral density (PSD) analysis and K-means clustering minimizes this possibility
656 and is essential to ensure our analysis remains focused exclusively on GABA-expressing neurons.

657 **Comparing pre-intervention and intervention cell-cell interaction strength**

658 Following step (i), the remaining dataset contains only traces associated with GABA neurons. In step
659 (ii), we assess the functional connectivity between the observed neurons using two measures of

pairwise association between calcium activity traces, namely covariance and a modified version of cross-correlation. The covariance between two traces $x = \{x_i\}$ and $y = \{y_i\}$, $i = 1,..,N$ is defined as

$$cov(x, y) = \frac{1}{N-1}\sum_i (x_i - \underline{x})(y_i - \underline{y}),$$

where $\underline{x} = \frac{1}{N}\sum_i x_i$ and $\underline{y} = \frac{1}{N}\sum_i y_i$, quantifying the strength of their linear association[27].

The modified cross-correlation, also accounting for lag and sign in cell-cell interactions, is termed *signed lagged cross-correlation* (SLxCorr) and is adapted from the works of Tsuyuzaki et al.[28] and Paparrizos & Gravano[29]. It is defined as

$$\mathrm{SLXCorr}(x,y) = \frac{R_{\tau_{max-N}}(x,y)}{\sqrt{R_0(x,x)R_0(y,y)}},$$

in which

$$\tau_{max} = \underset{\tau}{\mathrm{argmax}}\left(\left|\frac{R_{\tau-N}(x,y)}{\sqrt{R_0(x,x)R_0(y,y)}}\right|\right),$$

where $R_\tau = \begin{cases} \sum_{i=1}^{N-\tau-1} x_{i+\tau}.y_i & \text{for} \quad \tau \geq 0 \\ R_{-\tau}(y,x) & \text{for} \quad \tau < 0 \end{cases}$ represents cross-correlation with lag $\tau \in \{-N+1, ..., -1, 0, 1, ..., N-1\}$ with N as the length of x and y.

Using the above measures, we construct the corresponding covariance and SLxCorr matrices (see for an example Fig. 1**H&I**).

To evaluate changes in pairwise cell interactions between the pre-intervention and intervention phases, we compare the distributions of the covariance - and SLxCorr – derived connectivity weights using the Kolmogorov-Smirnov nonparametric statistical test[30,31]. This test is applied to each experimental trial where only the values of weights form the upper triangular entries (excluding the

678 diagonal) of the covariance and SLxCorr matrices are used to avoid duplication caused by
679 symmetry.

680 To account for variability across experiments, we combine the p-values obtained from individual
681 trials into a single p-value for each animal as shown in Fig. 1**J**. This is done using Fisher's Combined
682 Probability Test[32], providing an overall measure of the difference between the pre-intervention and
683 intervention experimental stages for each animal.

684 **Clustering analysis**

685 In step (iii), we apply agglomerative hierarchical clustering (using the average linkage criterion;
686 scikit-learn package in Python™) to classify cells based on the dissimilarity of their calcium activity,
687 given as

688 $$D(x, y) = 1 - \mathrm{SLXCorr}(x,y).$$

689 To determine the optimal number of clusters and robustness of clustering, we employed a
690 bootstrapping technique. This involved resampling (without replacement) 75% of the cells and
691 clustering the resulting dataset with different numbers of clusters (2, 3, and 4) using hierarchical or
692 K-means clustering with either the covariance or SLxCorr as the dissimilarity measure. This
693 resampling process was repeated 100 times.

694 For each resample dataset, we evaluate the clustering performance, using the Silhouette Coefficient
695 (SC)[33] which measures the cohesion within clusters and their separation, with values ranging from -1
696 (poor performance) to 1 (good performance). Results of the evaluation are given in Supplementary
697 Figs. 3-5, showing that the Silhouette Coefficient is significantly higher for 2 clusters compared to 3
698 or 4 clusters in the case of both hierarchical and K-means clustering.

699 **Modeling**

700 We build on our previously published modelling framework of MePD circuit[5] by incorporating
701 dynamic stimulation by UCN3 as observed experimentally (as shown in Fig. 3). To this end we

define UCN3 input into the populations of glutamatergic neurons and GABA interneurons with a strength given by the parameter γ. The activity of UCN3 during stimulation is approximated via sinusoidal function:

$$U_{stim}(t) = \gamma B + A\sin(2\pi f t) ,$$

where B and A are the baseline UCN3 activity and the amplitude, respectively, while the parameter f is the frequency of the sigmoid wave. We approximate UCN3 activity during restraint stress using two exponential functions:

$$U_{stress}(t) = \gamma(at\exp(-r_2 t) + b(1-\exp(-r_1 t))),$$

where the function initially increases with magnitude a then decreases to a plateau value given by the parameter b. The parameters r_1 and r_2 are responsible for the rate of increase of the first term and rate of decrease to a plateau in the second term.

Briefly, the model captures the dynamics of the MePD intracellular calcium activity of three populations: glutamatergic neuronal population (excitatory) and the populations of GABA interneurons and GABA efferent neurons (inhibitory). We build on our previous work[5] by assuming that excitatory (UCN3) input is provided to the populations of GABA interneurons and glutamate (Fig 7). Previous analysis of the model indicated that negative feedback between GABAergic and glutamatergic neuronal populations as well as glutamatergic self-excitation are critical mechanisms for inducing oscillatory dynamics[5]. However, providing glutamatergic inputs to both populations of GABA neurons result in a null phase difference between the populations. Therefore, we opted to provide glutamatergic input only to the population of GABA efferent neurons.

To investigate how the amygdala modulates the activity in the GnRH pulse generator, we couple the above-described MePD model to our KNDy network model, where the oscillatory dynamics of the KNDy acts as a proxy of LH pulsatility[18]. Here we couple the model via providing only inhibitory output from MePD GABA efferent neurons population to KNDy, as it was previously shown that glutamate plays a modulatory role to the MePD output rather than directly affecting the KNDy

network[5]. We then calibrate the coupled by reproducing the experimental results from Ivanova et al.[17] (Supplementary Fig. 6). Further modeling details, such as equations governing model dynamics and model parameter values, can be found in Supplementary Information. The simulations have been done in MATLAB (version R2023b).

Data Availability

Source data are provided with this paper. Further information that supports the findings of this study is available from the corresponding authors upon request.

Code Availability

The code for reproducing the data analysis (Python™), mathematical modeling (MATLAB), and figure generation for both the main text and Supplementary information, along with a test dataset, is publicly available at: https://github.com/mv-kr/MePD_GABA.

References

1. Yeo, S.-H., Kyle, V., Blouet, C., Jones, S. & Colledge, W. H. Mapping neuronal inputs to Kiss1 neurons in the arcuate nucleus of the mouse. *PLOS ONE* **14**, e0213927 (2019).
2. Moore, A. M., Coolen, L. M. & Lehman, M. N. Kisspeptin/Neurokinin B/Dynorphin (KNDy) cells as integrators of diverse internal and external cues: evidence from viral-based monosynaptic tract-tracing in mice. *Sci. Rep.* **9**, 14768 (2019).
3. Comninos, A. N. *et al.* Kisspeptin signaling in the amygdala modulates reproductive hormone secretion. *Brain Struct. Funct.* **221**, 2035–2047 (2016).
4. Lass, G. *et al.* Optogenetic stimulation of kisspeptin neurones within the posterodorsal medial amygdala increases luteinising hormone pulse frequency in female mice. *J. Neuroendocrinol.* **32**, e12823 (2020).
5. Nechyporenko, K. *et al.* Neuronal network dynamics in the posterodorsal amygdala: shaping reproductive hormone pulsatility. *J. R. Soc. Interface* **21**, 20240143 (2024).

751 6. Adekunbi, D. A. *et al.* Role of amygdala kisspeptin in pubertal timing in female rats. *PLOS ONE*
752 **12**, e0183596 (2017).
753 7. Ivanova, D. *et al.* Role of Posterodorsal Medial Amygdala Urocortin-3 in Pubertal Timing in
754 Female Mice. *Front. Endocrinol.* **13**, (2022).
755 8. Adekunbi, D. A. *et al.* Kisspeptin neurones in the posterodorsal medial amygdala modulate
756 sexual partner preference and anxiety in male mice. *J. Neuroendocrinol.* **30**, e12572 (2018).
757 9. Wu, Y. E. *et al.* Neural control of affiliative touch in prosocial interaction. *Nature* **599**, 262–267
758 (2021).
759 10. Ivanova, D. *et al.* Urocortin3 in the Posterodorsal Medial Amygdala Mediates Stress-induced
760 Suppression of LH Pulsatility in Female Mice. *Endocrinology* **162**, 1–14 (2021).
761 11. McIntyre, C. *et al.* GABA Signaling in the Posterodorsal Medial Amygdala Mediates Stress-
762 induced Suppression of LH Pulsatility in Female Mice. *Endocrinology* **164**, 1–11 (2023).
763 12. Keshavarzi, S., Sullivan, R. K. P., Ianno, D. J. & Sah, P. Functional Properties and Projections
764 of Neurons in the Medial Amygdala. *J. Neurosci.* **34**, 8699–8715 (2014).
765 13. Choi, G. B. *et al.* Lhx6 delineates a pathway mediating innate reproductive behaviors from the
766 amygdala to the hypothalamus. *Neuron* **46**, 647–660 (2005).
767 14. Bian, X. Physiological and morphological characterization of GABAergic neurons in the medial
768 amygdala. *Brain Res.* **1509**, 8–19 (2013).
769 15. Lewis, K. *et al.* Identification of urocortin III, an additional member of the corticotropin-releasing
770 factor (CRF) family with high affinity for the CRF2 receptor. *Proc. Natl. Acad. Sci. U. S. A.* **98**,
771 7570–7575 (2001).
772 16. Shemesh, Y. *et al.* Ucn3 and CRF-R2 in the medial amygdala regulate complex social
773 dynamics. *Nat. Neurosci.* **19**, 1489–1496 (2016).
774 17. Ivanova, D., Li, X.-F., McIntyre, C. & O'Byrne, K. T. Posterodorsal Medial Amygdala Urocortin-3,
775 GABA, and Glutamate Mediate Suppression of LH Pulsatility in Female Mice. *Endocrinology*
776 **164**, 1–13 (2023).
777 18. Voliotis, M. *et al.* The Origin of GnRH Pulse Generation: An Integrative Mathematical-
778 Experimental Approach. *J. Neurosci.* **39**, 9738–9747 (2019).

19. Hochgerner, H. *et al.* Neuronal types in the mouse amygdala and their transcriptional response to fear conditioning. *Nat. Neurosci.* **26**, 2237–2249 (2023).
20. Li, Y. *et al.* Neuronal Representation of Social Information in the Medial Amygdala of Awake Behaving Mice. *Cell* **171**, 1176-1190.e17 (2017).
21. Paxinos, G. & Franklin, K. B. J. *Paxinos and Franklin's the Mouse Brain in Stereotaxic Coordinates*. (2019).
22. Steyn, F. J. *et al.* Development of a Methodology for and Assessment of Pulsatile Luteinizing Hormone Secretion in Juvenile and Adult Male Mice. *Endocrinology* **154**, 4939–4945 (2013).
23. Vidal, A., Zhang, Q., Médigue, C., Fabre, S. & Clément, F. DynPeak: An Algorithm for Pulse Detection and Frequency Analysis in Hormonal Time Series. *PLOS ONE* **7**, e39001 (2012).
24. Yang, J. A. *et al.* Acute Psychosocial Stress Inhibits LH Pulsatility and Kiss1 Neuronal Activation in Female Mice. *Endocrinology* **158**, 3716–3723 (2017).
25. Pnevmatikakis, E. A. & Giovannucci, A. NoRMCorre: An online algorithm for piecewise rigid motion correction of calcium imaging data. *J. Neurosci. Methods* **291**, 83–94 (2017).
26. Friedrich, J., Zhou, P. & Paninski, L. Fast online deconvolution of calcium imaging data. *PLOS Comput. Biol.* **13**, (2017).
27. Rice, J. A. *Mathematical Statistics and Data Analysis*. (Thomson/Brooks/Cole, Belmont, CA, 2007).
28. Tsuyuzaki, K. *et al.* WormTensor: a clustering method for time-series whole-brain activity data from C. elegans. *BMC Bioinformatics* **24**, 254 (2023).
29. Paparrizos, J. & Gravano, L. k-Shape: Efficient and Accurate Clustering of Time Series. *SIGMOD Rec* **45**, 69–76 (2016).
30. Kolmogorov, A. Sulla determinazione empirica di una legge didistribuzione. *Giorn Dellinst Ital Degli Att* **4**, 89–91 (1933).
31. Smirnoff, N. On the estimation of the discrepancy between empirical curves of distribution for two independent samples. *Bull Math Univ Moscou* **2**, 16 (1939).
32. Fisher, S. R. A. *Statistical Methods for Research Workers*. (Oliver & Boyd, 1970).
33. Rousseeuw, P. J. Silhouettes: A graphical aid to the interpretation and validation of cluster

analysis. *J. Comput. Appl. Math.* **20**, 53–65 (1987).

Acknowledgements

We thank Ms Sumi Mathew for her technical support with genotyping mice.

S.F., M.V., K.T.A., K.T.O., X.F.L. gratefully acknowledge the financial support of BBSRC via grants BB/W005913/1 (KCL), BB/W005883/1 (Exeter) and BB/S019979/1. KTA gratefully acknowledges the financial support of the EPSRC via grant EP/T017856/.

Contributions

J.Y. contributed data acquisition and data analysis, S.F. contributed data analysis, K.N. contributed modeling, M.V. contributed managing data analysis, X.F.L. contributed managing data acquisition, H.Y. contributed data acquisition, Y.L. contributed data acquisition, J.Y. contributed data acquisition, O.H. contributed data acquisition, R.D.B. contributed data acquisition, K.T.O., K.T.A. and M.V. contributed to managing the project. All authors contributed to writing the manuscript.

Competing interests

The authors declare no competing interests.

Corresponding author

Correspondence and requests for materials should be addressed to Krasimira Tsaneva-Atanasova (K.Tsaneva-Atanasova@exeter.ac.uk), Kevin T. O'Byrne (kevin.o'byrne@kcl.ac.uk), Margaritis Voliotis (m.voliotis@exeter.ac.uk).

Open Access

For the purpose of open access, the authors have applied a 'Creative Commons Attribution (CC BY) licence to any Author Accepted Manuscript version arising from this submission.